Proceedings of the ASME 2010 3rd Joint US-European Fluids Engineering Summer Meeting and 8th International Conference on Nanochannels, Microchannels, and Minichannels
FEDSM-ICNMM2010
August 1-5, 2010, Montreal, Canada

FEDSM-ICNMM2010-30711

FLOW AND HEAT TRANSFER OF MICRO-TUBE BANK

Yasuo Koizumi
Shinshu University
Ueda, Nagano, Japan

Atsushi Katsuta
Kogakuin University
Shinjuku, Tokyo, Japan

Hiroyasu Ohtake
Kogakuin University
Shinjuku, Tokyo, Japan

ABSTRACT

Heat transfer and flow behavior in a mini-tube bank was examined. The tube bank was simulated with wires of 1 mm diameter. The wires were arranged in the 5×5 in-line array and the 5×5 staggered array with the arranging pitch = 3. Experiments were performed in the range of the tube Reynolds number Re = 4 ~ 3,500. Numerical analyses were also performed with the commercial CFD code of STAR-CD. The heat transfer coefficient of the tube of the first row was well expressed with the existing heat transfer correlations. In the case of the in-line array, unlike usual sized tube banks, the measured heat transfer coefficients of the tubes after the second row were lower than those of the first row and the difference between those increased as the Reynolds number was increased. At approximately Reynolds number ≃ 50, the difference turned to decrease; the heat transfer coefficients initiate to recover to the first row value. Then, the heat transfer coefficient in the rear row became larger at approximately Re ≃ 1,000 than that of the first row. In the case of the staggered array, the decrease in the heat transfer coefficient in the rear row was smaller than that in the case of the in-line array. The recovery of the heat transfer coefficient to the first row value started at a little bit lower Reynolds number and it exceeded the first row value at approximately Re ≃ 700. The flow visualization results and also the STAR-CD analytical results indicated that when the Reynolds number was low, the wake region of the preceding tube was stagnant. This flow stagnation caused the heat transfer deterioration in the front part of the rear tube, which resulted in the lower heat transfer coefficient of the rear tube than that of the first row. As the Reynolds number was increased, the flow state in the wake region changed from the stagnant condition to the more disturbed condition by periodical shedding of the Karman vortex. This change caused the recovery of the heat transfer in the front region of the rear tube, which resulted in the recovery of the heat transfer coefficient of the rear tube.

INTRODUCTION

Heat exchangers are one of the main pieces of equipments for engineering systems such as power plants, chemical plants and so on. They have been investigated by many researchers from many aspects. An effort has been made to improve the efficiency of heat exchangers pursuing more efficient energy use. One of these efforts is to adopt small diameter tubes and small fins.

Kamisaka et al. [1] examined the effect of micro needle fins formed on the tubes of the heat exchanger on the heat transfer and developed the correlation of the heat transfer coefficient.

A heat transfer coefficient of flow that crosses a tube increases as the tube diameter is decreased. It implies that when the tube diameter and the size of the heat exchanger are scaled down, the overall heat transfer coefficient and the efficiency would be enhanced. Kasagi et al. [2, 3] examined micro-bare tube heat exchangers to improve the heat exchanger efficiency. They provided the design guide line for these micro heat exchangers from numerical analyses.

The flow behavior through a tube bank is so complicated that it is virtually impossible to predict heat transfer and pressure drop by a numerical analysis [4]. Therefore, an experimental approach is alternative and a lot of experimental data are available in the literature. In the turbulent condition of the tube bank, turbulence created by the preceding row has an

effect on the heat transfer of the following row. Heat transfer is usually improved as the tube row proceeds deep [5, 6]. However, when the diameter of the tubes is scaled down, the Reynolds number of the cross-flow also becomes low. Therefore, the effect of the disturbance created by the preceding row may become different.

When the tube size is scaled down to miniature size to improve the heat transfer coefficient, the flow becomes laminar. The heat transfer coefficient of a tube bank is 50 % lower than that of the first row [4]. Mochizuki et al. [7] and Yagi and Mochizuki [8] examined heat transfer and pressure drop of the miniature size rod bank. They reported that the heat transfer coefficient of the rod bank could be larger than that of the single rod in some case. It was pointed out that the heat transfer coefficient of the rod bundle is highly sensitive to the flow state and it was complicatedly affected by the rod arrangement.

Koizumi et al. [9 - 11] have examined the heat transfer and the flow behavior of a tube bank that was composed of 1 mm diameter wires. They reported that the heat transfer coefficient after the second row was lower than that of the first row because the wake region was stagnant. As the Reynolds number was increased, the heat transfer coefficient began to recover to the first row value at a certain Reynolds number. They accounted that the flow state in the wake region gradually changed from the stagnant condition to the more disturbed condition.

It is considered that flow and heat transfer data on the mini-size tube bank are still required to get better design guidelines for the micro heat exchangers. It seems important to examine the flow state in the wake region between tubes.

The present paper follows Koizumi et al.'s research. Further experimental and analytical work has been performed on the heat transfer and the flow behavior in the mini tube bank. The tube bank was composed of 1 mm diameter wires in a 30 mm W × 15 mm H or a 15 mm W × 15 mm H rectangular flow channel. The arrays tested were a 5 × 5 in-line array and a 5 × 5 staggered array. Fluid used in the experiments was distilled water. The test condition covered the Reynolds number of the tubes from 4 to 3,500. The Reynolds number corresponded to the flow velocity of 0.0043 m/s ~ 2.6 m/s in the channel. Experimental results were also analyzed with a commercial analytical code of STAR-CD.

EXPERIMENTAL APPARATUS AND TEST PROCEDURES

Experimental Apparatus

An apparatus used in the present study is schematically shown in Fig. 1. It consists of a water storage tank, a circulation pump, rotameters, a calming grid at the inlet of the test section, a test section, rod bundles in the test section and a low-voltage DC current supply system. Test fluid is distilled water.

The test section is made of transparent Plexiglas. The length is 470 mm and the cross-section is rectangular. Two test sections are prepared. One is 30 mm wide and 15 mm high and another is 15 mm wide and 15 mm high. The test section is placed horizontally. It has the calming grid at the inlet that is composed of 3 mm cell-size octagonal pipes of 200 mm long. The test tube bank is located at 100 mm downstream from the calming grid.

The tubes are simulated with a 1 mm diameter nickel wire. The wires (tubes) are oriented vertically. Water flow crosses the wires perpendicularly. Two-types of rod arrangement are adopted. One is in-line array and another is staggered array. In the case of the in-line array, wires are arranged in five rows perpendicularly to flow and five lines parallel to flow; 5 × 5. In the case of the staggered array, wires are arranged in five rows and eleven lines as shown in Fig. 2. The staggered array is called the 5 × 5 staggered array in the present paper hereafter. The spacing pitch S/D of the tubes in the present experiments is fixed at 3, where D is the wire diameter and S is the distance between the centers of the neighbouring wires.

Water pumped out from the water storage tank flows into the inlet plenum of the test section through the rotameter. Then, it flows in the test section and returns to the tank. The temperature of water is measured with K-type thermocouples at the inlet and the outlet of the test section. Experiments are performed under atmospheric pressure and room temperature. The thermocouples and the rotameters were calibrated prior to the experiments.

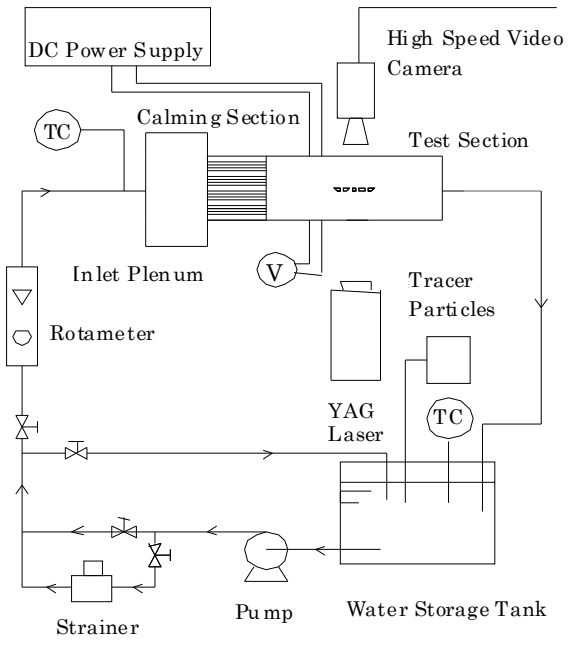

Fig. 1 Experimental Apparatus

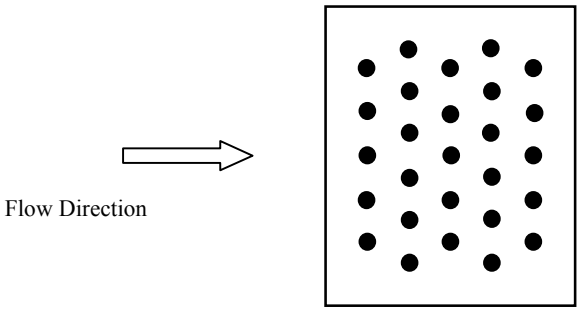

Fig. 2 Rod Arrangement of Staggered Array

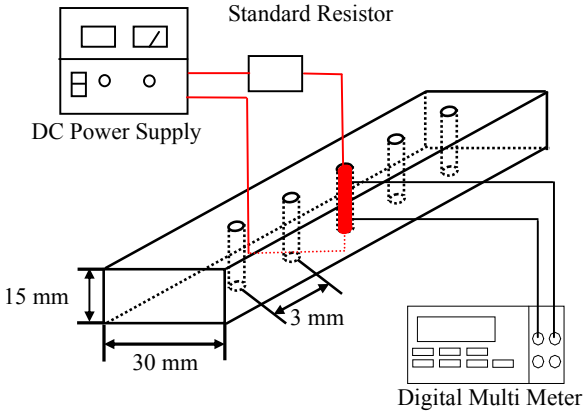

Fig. 3 Details of Rod Heating and Temperature Measurement

Experimental Procedures

Distilled water in the water storage tank was cleaned with a strainer prior to each experiment by circulating water through a bypass line. After water was cleaned, the bypass line was isolated. Then, the flow was directed to the test section through the flow meter and the temperature measuring section.

Two types of experiments were conducted in the present experiments; heart transfer experiments and flow visualization experiments.

Heat transfer experiments

The details of rod heating and rod temperature measurement are illustrated in Fig. 3. The figure shows the center line of the rod bundle. Only one rod (Ni wire) in the center line was heated.

Low voltage DC current was supplied to the heating rod. The rod was heated by joule heating. Two alumel wires of 0.05 mm diameter were spot-welded on the heated rod with an interval of 6 mm. The DC current that was supplied for the rod was derived by measuring the voltage through a standard resistor. Voltage between the spot-welded alumel wires was also measured. The electric resistance of the rod (Ni wire) was calculated from the current and the voltage. Electric power supplied for the wire was derived from the current and the electric resistance, and then the heating rate of the wire and the surface heat flux were calculated. By referring to the relation between the electric resistance of the rod and the rod temperature that had been calibrated prior to the experiment, mean rod temperature was obtained.

For the fixed flow rate, five experiments were iterated, such as only the first wire was heated, only the second wire was heated next, then only the third wire was heated, and so on.

The water velocity at the upstream of the rod bundles in the test section; the approaching velocity, was varied in the range of 0.0043 ~ 2.6 m/s. The flow conduit Reynolds number $Re = uD_{hy}/\nu$ corresponding to those flow velocities was in a range of 92 ~ 56,000. The rod Reynolds number $Re = u_{max}D/\nu$ was in a range of 4 ~ 3,500. Here, D is the wire diameter, D_{hy} is the hydraulic diameter of the flow channel, u is the approaching velocity u_{max} is the maximum velocity in the rod bundle and ν is the kinematic viscosity of water.

Flow visualization experiments

The flow visualization experiment setup is shown in Fig. 4. Fluorescent dye of 6 μm diameter particles was dissolved in distilled water as tracer particles. A YAG laser sheet was emitted from the side of the tube bank. The visualized flow image was recorded from the top of the test section by a high speed video camera with a frame rate of 125 ~ 1000 f/s. The recorded pictures went through the binary digitizing process, and then the velocity field was determined by the PIV or PTV method.

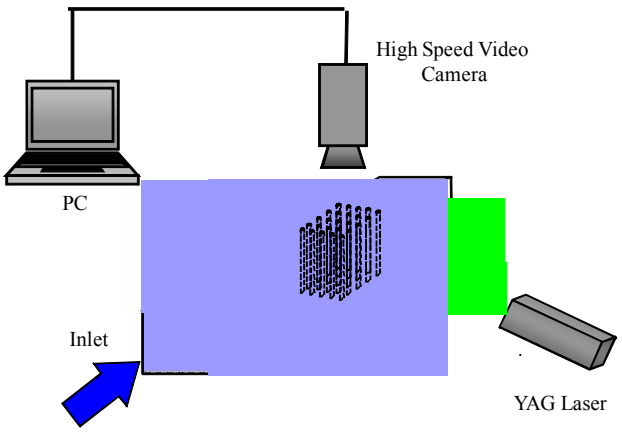

Fig. 4 Flow Visualization Experiment Setup

Table 1 Analytical Conditions

Fluid	H_2O
Rod Diameter	1 mm
Pitch	3
Fluid Temperature	300 K
Heating Surface Temperature	305 K
Time Domain	Transient
Analysis Time	0.1~10 S
Time Step	0.00005~0.01 S
Rod Reynolds number	9 ~ 800
Total Cell Number	480,000

NUMERICAL ANALYSES WITH STAR-CD

The flow field of the rod bank of the 5×5 in-line and staggered array was analyzed two-dimensionally with the STAR-CD Ver. 3.2 code by CD-Adapco. Fluid was water as in the experiments. The analytical conditions are shown in Table 1. The rod diameter D was 1 mm. The rod arrangement pitch was 3 mm. Any turbulent model was not adopted since the flow speed was slow; the rod Reynolds number = 9 ~ 800 in the analyses.

RESULTS AND DISCUSSIONS

Results of Heat Transfer Experiments

The results of the heat transfer experiments of the 5 × 5 in-line array are presented in Fig. 5. In the figure, the Nusselt number is

$$Nu = \frac{hD}{k_f} \quad . \tag{1}$$

Here, h is the heat transfer coefficient, D is the rod diameter and k_f is the thermal conductivity of water evaluated at the film temperature $T_f = (T_m + T_w)/2$, where $T_m = (T_{in} + T_{out})/2$ and T_w is the average rod surface temperature. The temperatures T_{in} and T_{out} are the fluid temperature at the inlet and the outlet of the rod bundle.

The heat transfer coefficient h is calculated from the measured heat flux q and the measured temperatures of the rod and water; T_r and T_w (= T_{in} in the present experiments), respectively as

$$h = \frac{q}{T_r - T_w} \quad . \tag{2}$$

The Reynolds number is defined as

$$Re = \frac{u_{max} D}{\nu_f} \quad . \tag{3}$$

In Eq. (3), u_{max} is the maximum velocity in the tube bank and the symbol ν_f is the kinematic viscosity of water at the film temperature.

A solid line in Fig. 5 expresses the value calculated with the McAdams correlation (Reference [5]) for the heat transfer coefficient of the cross-flow of a single rod

$$Nu = \frac{hD}{k_f} = C_m \, Re^{nm} \, Pr^{1/3} \quad . \tag{4}$$

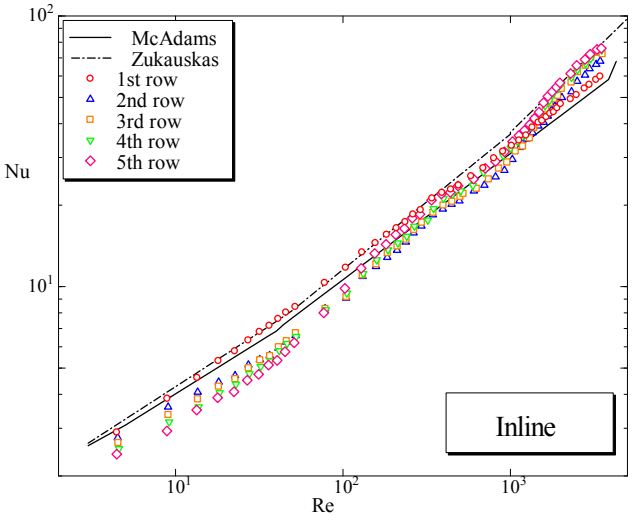

Fig. 5 Heat Transfer Coefficients of 5 ×5 In-line Array

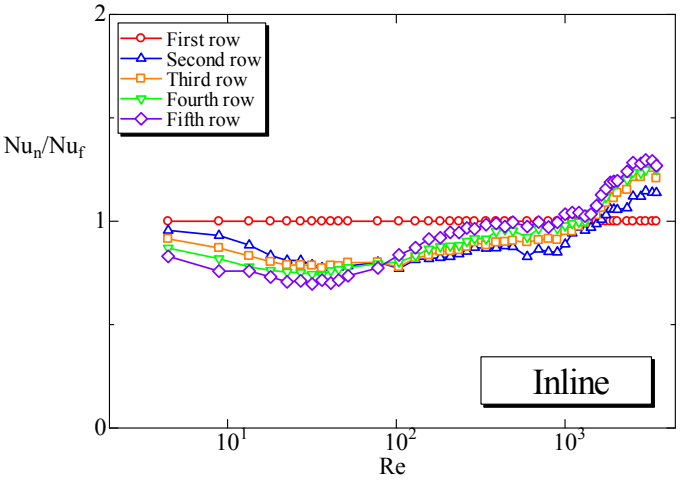

Fig. 6 Normalized Heat Transfer Coefficients of 5 ×5 In-line Array

In Eq. (4), Pr is the Prandtl number at the film temperature. The constant C_m and the exponent n_m for the Reynolds number are dependent on the Reynolds number. In the present case, C_m = 0.911 ~ 0.683 and n_m = 0.385 ~ 0.466.

Similarly, a chain line with one dot expresses the value calculated with the Zukauskas correlation (Reference [12]) for the heat transfer coefficient of the cross-flow of a single rod

$$Nu = \frac{hD}{k_f} = C_z \, Re^{n_z} \, Pr^{0.37} \left(\frac{Pr}{Pr_w} \right)^{0.25} \quad . \qquad (5)$$

In the equation, Pr_w is the Prandtl number at the rod temperature. The constant C_z and the exponent n_z for the Reynolds number are dependent on the Reynolds number. In the present case, C_z = 0.51 ~ 0.75 and n_z = 0.4 ~ 0.5.

The Nusselt number of each row is divided by the value of the first row and its result is plotted against the Reynolds number in Fig. 6. In Fig. 5, the first row results are well expressed with the correlations; Eqs. (4) and (5). In the low Reynolds number region, the Nusselt numbers in the rear rows are lower than the first row values. It is clearly observed in Fig. 6. This result is different from the textbook knowledge about the tube bank that the heat transfer coefficient increases as the row goes downstream in first ~ 10 rows. When the Reynolds number is lower than approximately 50, the difference between the first row Nusselt number and the rear row values becomes large as the row goes downstream and as the Reynolds number increases. At Re ≃ 50, the difference between the first row values and the rear row values begins to decrease; the deterioration of the heat transfer in the rear rows begins to recover to the first row value. The recovery with an increase in the Reynolds number is faster in the lower row. At Re ≃ 100, the order of the magnitude of the Nusselt number of the rear rows changes and the Nusselt number becomes large as the row goes downstream. The Nusselt number at the fifth row reaches the first row value at Re ≃ 400, and it exceeds the first row value at Re ≃ 1,000. The Nusselt number at the second row exceeds the first row value at Re ≃ 2,000.

Figure 7 is the Nusselt numbers of the 5 × 5 staggered array. The values are divided by the first row values and results are presented in Fig. 8. The general trends observed in the figures are similar to those in Figs. 5 and 6 of the 5 × 5 in-line array. The decrease in the Nusselt number from the first row value in the rear row region is a little bit smaller than that in the in-line array case. The difference of the Nusselt number among the rear rows is also smaller than that in the in-line array case. The Nusselt numbers in the rear rows become larger at the smaller Reynolds number; Re ≃ 700, than that in the in-line array case.

It should be noticed that the heat transfer coefficient of the rod in the rear rows is smaller than that of the first row in the low Reynolds number whether the rod arrangement is staggered or in-line. The fact is different from the knowledge about the usual-sized tube bank.

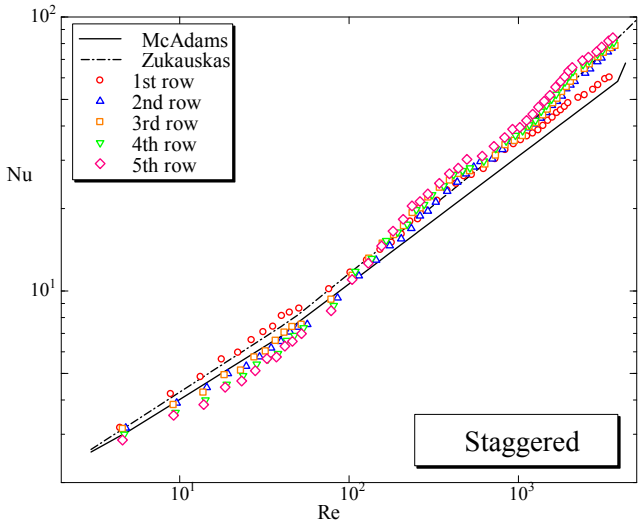

Fig. 7 Heat Transfer Coefficients of 5 ×5 Staggered

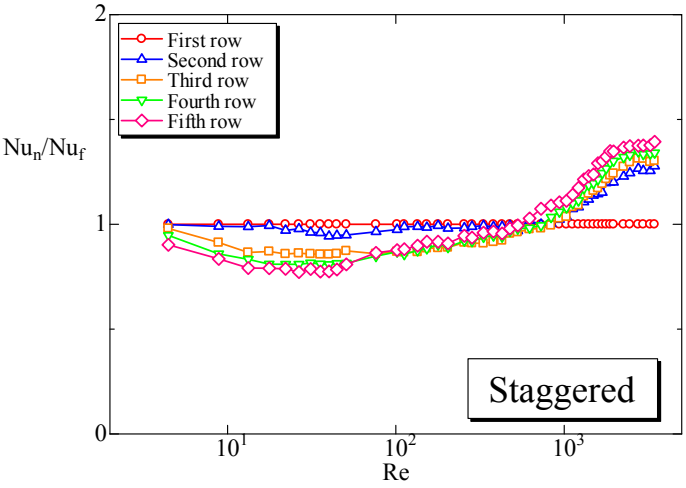

Fig. 8 Normalized Heat Transfer Coefficients of 5 ×5 Staggered Array

Results of Flow Visualization Experiments

The flow images recorded with a high speed video camera were binary-digitized. Then, by using the PTV method, flow field was obtained. Flow fields so obtained are presented in Figs. 9 ~ 11. Figure 9 expresses a flow state between the first row and the second low at Re = 9. There seems to be no vortex there and the wake is closed. The wake becomes stagnant and the velocity in the wake is slower than the approaching velocity. It implies that the heat transfer in the front region of

the rod in the second row is deteriorated. It causes the smaller heat transfer coefficient of the second row rod than that of the first row rod.

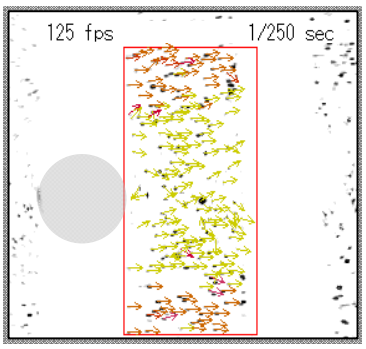

Fig. 9 Flow Field by PTV (Re = 9, 1st – 2nd Row)

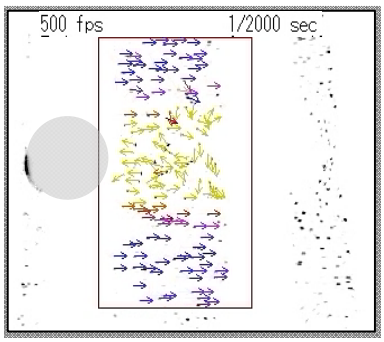

Fig. 10 Flow Field by PTV (Re = 80, 1st – 2nd Row)

Figure 10 exhibits a flow state between the first row and the second low at Re = 65. The wake behind the first row seems still stagnant although twin vortices steadily exist there. It also implies that the flow stagnation in the wake region results in the lower heat transfer coefficient than that in the first row.

When the Reynolds number is increased to 200, periodical Karman vortex shedding is observed in the wake of the first row as shown in Fig. 11 (a). This disturbed situation appears to cause the initiation of the recovery of the heat transfer in the front region of the rod in the second row. It resulted in the recovery of the heat transfer coefficient of the second row rod. As presented in Fig. 11 (b), the vortex shedding is more vigorous in the wake of the forth row than that in the wake of the first row. This difference of the wake situation seems to be reflected on the faster and larger recovery of the heat transfer coefficient in the deeper row.

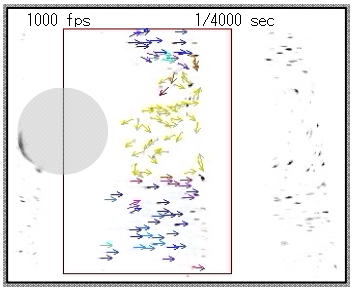

(a) 1st – 2nd Row

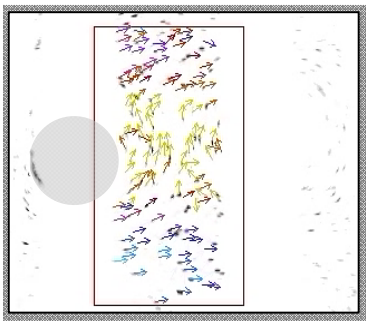

(b) 4th – 5th Row

Fig. 11 Flow Field by PTV (Re = 200)

Results of Numerical Analyses with STAR-CD

The flow fields that were predicted by the STAR-CD code are illustrated in Fig. 12 ~14. The cases of the figures are for the 5 × 5 in-line array and for the Reynolds number = 85, 200 and 800, respectively. When Re = 85, all wakes are stagnant as was observed in the experiments; Fig. 10. When Re =200 in Fig. 13, the Karman vortices are clearly observed. The flow stagnation in the wake has disappeared. The deeper the row is, the more vigorous the vortices are. This situation is the same as that observed in the experiments in Fig. 11. When the Reynolds number is further increased to 800, the wake behind the fifth row is highly agitated. The rod in fifth row is surrounded by largely disturbed flow. This seems to cause the recovery of the heat transfer coefficient of the fifth row rod to the first row value and exceed it as shown in Figs. 7 and 8.

Predicted heat transfer coefficient distributions around a rod are presented in Fig. 15. The distribution profiles of the first row are approximately similar in all cases irrespective of the Reynolds number. However, when Re = 85, there is a large dip at the stagnation point of the second row and the fifth row. When the Reynolds number is increased to 200, the large dip of the heat transfer coefficient at the stagnation point of the

second and the fifth row has disappeared. This is caused by the flow situation change as shown in Fig, 13.

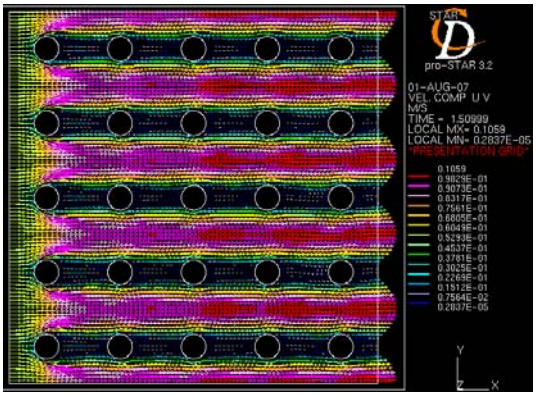

Fig. 12 Flow field by STAR-CD (Re = 85)

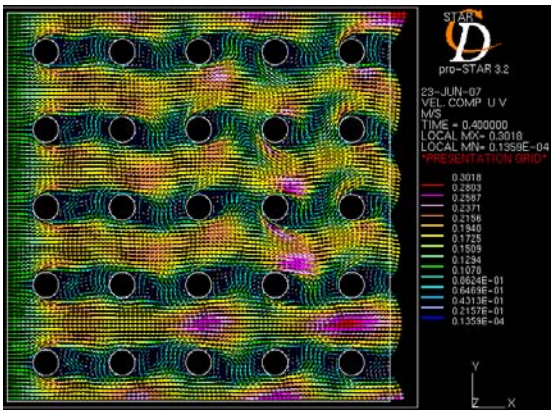

Fig. 13 Flow field by STAR-CD (Re =

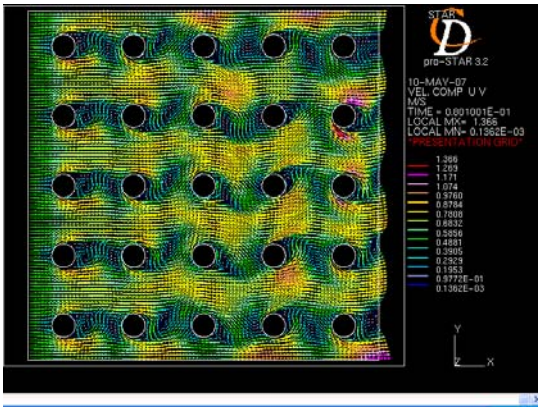

Fig. 14 Flow field by STAR-CD (Re = 800)

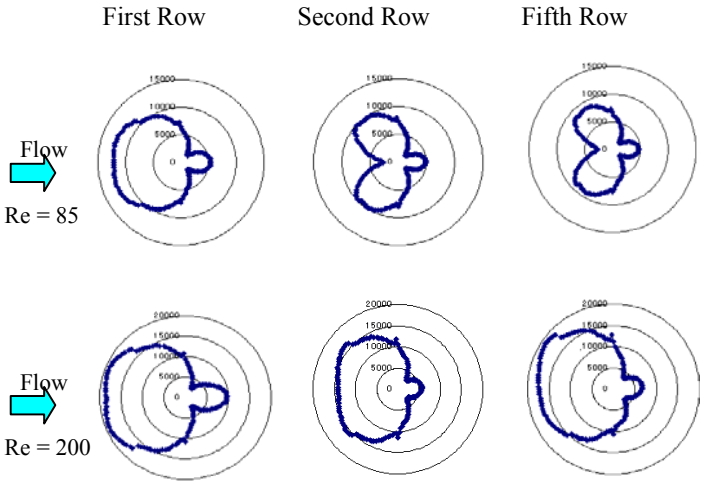

Fig. 15 Local Heat Transfer Coefficients

It is confirmed from these that the heat transfer coefficient variation of the rod in the rear rows of the first row with the variation of the Reynolds number is the result of the state change of the wake as the Reynolds number variation; when the Reynolds number is low; it means that the flow velocity is low, the wake behind the preceding row is stagnant and as the flow velocity is increased, the wake region becomes largely disturbed, which resulted in the variation of the heat transfer coefficient with the Reynolds number. It has not been noticed since the Reynolds number in the usual-sized tube bank is usually large. When the size of the tube bank is scaled down, the rod Reynolds number becomes very low and the flow state behind the rod becomes different from that of the high Reynolds number. Since the flow state in the wake is dependent on the Reynolds number, the heat transfer of the rod bundle is affected by the Reynolds number.

CONCLUSIONS

Heat transfer and flow behavior in the mini-tube bank was examined. The tube bank was simulated with wires of 1 mm diameter. The wires were arranged in the 5×5 in-line array and in the 5×5 staggered array. Experiments were performed in the range of the tube Reynolds number Re = 4 ~ 3,500. Numerical analyses were also performed with the commercial CFD code of STAR-CD. Conclusions obtained are as follows.

(1) The heat transfer coefficient of the tube of the first row was well expressed with the existing heat transfer correlations.

(2) In the case of the in-line array, unlike the usual sized tube banks, the measured heat transfer coefficients of the tubes after the second row were lower than those of the first row and the difference between those increased as the Reynolds number was increased. At approximately Reynolds number =50, the

difference turned to decrease; the heat transfer coefficients initiated to recover to the first row value. When the Reynolds number exceeded approximately 1,000, then heat transfer coefficient in the rear row became larger than that of the first row. In the case of the staggered array, the decrease in the heat transfer coefficient in the rear row was smaller than that in the case of the in-line array. The recovery of the heat transfer coefficient to the first row value started at a little bit lower Reynolds number and it exceeded the first row value at approximately Re = 700.

(3) The flow visualization results and also the STAR-CD analytical results indicated that when the Reynolds number was low, the wake region of the preceding tube was stagnant. This flow stagnation caused the heat transfer deterioration in the front part of the rear tube, which resulted in the lower heat transfer coefficient of the rear tube than that of the first row. As the Reynolds number was increased, the flow state in the wake region changed from the stagnant condition to the more disturbed condition by periodical shedding of the Karman vortex. This change caused the recovery of the heat transfer in the front region of the rear tube, which resulted in the recovery of the heat transfer coefficient of the rear tube.

REFERENCES

[1] Kamisaka, M., Aoki, Y. and Ueda, S., 1988. "Heat Transfer Characteristics of Pin-Finned Heat Exchangers", Proc. 25th National Heat Transfer Symp. of Japan, Vol. 1, 181-183.

[2] Kasagi, N., Shikazono, N., Suzuki, Y. and Oku, T., 2003. "Assessment of High-Performance Micro Bare-Tube Heat Exchangers for Electronic Equipment Cooling", Proc. 1st Int. Symp. on Process Intensification and Miniaturization, Univ. of Newcastle upon Tyne, UK, CD-ROM.

[3] Kasagi, N., Shikazono, N., Suzuki, Y. and Oku, T., 2003. "Optimal Design and Assessment of High-Performance Micro Bare-Tube Heat Exchangers", Proc. 4th Conf. on Compact Heat Exchangers and Enhancement Technology for the Process Industries, Crete Island, Greece, 241 - 246.

[4] Özisik, M. N., 1987. "Basic Heat Transfer", Robert E. Krieger Publishing Co., 278 - 282.

[5] Katto, Y., 1964. "Heat Transfer Introduction", Yokendo Co., 155 - 156, 153 - 160.

[6] Rohsenow, W. M., Hartnett, J. P. and Ganic, E. N., 1973. "Handbook of Heat Transfer Fundamentals", McGraw-Hill Book Co., 8-130 - 8-133.

[7] Mochizuki, S., Yagi, Y. and Hara, T., 1992. "Heat Transfer and Pressure Drop Performance of Wire-Fin Surfaces", Trans. JSME, Vol. 58, No. 566, 3729 -3734.

[8] Yagi, Y. and Mochizuki, S., 1994. "Empirical Correlation for Heat Transfer and Pressure Drop Characteristics of Thin Wire Fin Surfaces", Trans. JSME, Vol. 60, No. 575, 2518 - 2523.

[9] Koizumi, Y., Ohtake, H. and Okuyama, T., 2006. "Study on Heat Transfer and Flow Behavior of Mini-Tube Bank for Micro Heat Exchanger", 2006 ASME International Mechanical Engineering Congress and Exposition, IMECE2006-14626.

[10] Arai, M., Koizumi, Y. and Ohtake, H., 2007. "Study on Heat Transfer and Flow Analysis of 5×5 and 5×1 Mini-Tube Bank of Micro Heat Exchanger, 2007 ASME International Mechanical Engineering Congress and Exposition, IMECE2007-41608.

[11] Koizumi, Y., Katsuta, A., Arai, M. and Ohtake, H., 2008. " Study on Heat Transfer and Flow Behavior of Micro Heat Exchanger Composed of Mini-Tubes", 7th JSME – KSME Thermal and Fluids Engineering Conf., CD-ROM, A334.

[12] JSME Data Book: Heat Transfer 5th Ed., 2009. JSME, 34 - 35.